JOURNAL OF CATALYSIS 140, 585–600 (1993)

# Studies of Gas Adsorption on ZnO Using ESR, FTIR Spectroscopy, and MHE (Microwave Hall Effect) Measurements

BYUNG-KI NA,[1] ARDEN B. WALTERS,* AND M. ALBERT VANNICE[2]

*Department of Chemical Engineering, The Pennsylvania State University, University Park, Pennsylvania 16802; and *Florida Power and Light Company, P.O. Box 14000, Juno Beach, Florida 33408-0420*

Received August 25, 1992; revised November 24, 1992

This paper describes the application of a new technique—Microwave Hall Effect (MHE) measurements—to measure electron mobilities and to determine the effect of adsorption on electron densities of powders. Conduction electron densities calculated from microwave measurements of both mobilities and conductivities, as well as ESR spectroscopy and chemisorption measurements, have been applied to characterize high-surface-area ZnO (up to 30 $m^2/g$) samples before and after exposure to $O_2$, $CO_2$, CO, and $H_2$. Evacuation at 673 K removed lattice oxygen to produce paramagnetic lattice vacancies, $(V_0^{\cdot})^{\cdot}$, and an approximately equal number of conduction electrons, $e^-$. Adsorption of $O_2$ decreased both species and created an $O_2^-$ species, but a larger quantity of $O_2$ also adsorbed and appeared to reoxidize the surface and remove neutral $V_0$ sites. Reversible CO adsorption occurred which had little effect on $(V_0^{\cdot})^{\cdot}$ and $e^-$; however, CO adsorption on an oxygen-precovered surface reestablished $(V_0^{\cdot})^{\cdot}$ and $e^-$ species and decreased the $O_2^-$ species. After this step, very weak carbonate bands were observed using DRIFTS. $CO_2$ adsorption on ZnO after evacuation at 673 K decreased the $e^-$ and $(V_0^{\cdot})^{\cdot}$ concentrations equally, while much smaller decreases of each species occurred after $CO_2$ adsorption on an oxygen-precovered surface, although $O_2^-$ species were unaffected. This showed that $CO_2$ does not react with adsorbed $O_2^-$ species, but can interact with both $(V_0^{\cdot})^{\cdot}$ and conduction electrons at sites not covered by molecular oxygen. 

## INTRODUCTION

It is well established that ZnO develops a strong ESR signal at $g = 1.961$ after evacuation at 673 K with an intensity that is decreased by the subsequent adsorption of oxygen at 300 K while a new ESR signal is created at $g = 2.003$. The signal at $g = 1.961$ has been assigned to paramagnetic oxygen vacancies in the lattice (*1–3*), while the signal at $g = 2.003$ has usually been assigned to adsorbed $O_2^-$ (*1, 4–6*). The oxygen-vacancy signal is believed to correlate with the bulk electrical properties of zinc oxide. ZnO is an intrinsic n-type semiconductor and its electrical properties can be changed by different treatment conditions; for example, DC conductivity measurements have shown that the conductivity increases after ZnO is heated in vacuum and it decreases after exposure to oxygen (*7–9*).

Previous studies have used either ESR spectroscopy or DC/AC conductivity measurements, but the application of these two characterization methods to the same sample has not been made, nor has the gas uptake been simultaneously determined in this earlier work. Furthermore, because the assumption of constant mobility may not hold true, even at relatively low carrier densities as reported earlier for ZnO after various pretreatments (*11*), it is also important to measure both charge carrier mobility and conductivity to accurately determine electron density. In this study, Microwave Hall Effect (MHE) measurements, conducted with a modified ESR spectrometer attached to a UHV/gas handling system, allowed electron mobility and conductivity along with

[1] Present address: Department of Chemical Engineering, Carnegie Mellon University, Pittsburgh, PA 15213.

[2] To whom correspondence should be addressed.



0021-9517/93 $5.00

ESR and adsorption measurements to be made on the same sample after any chosen pretreatment. The details of the system and the equipment modifications are described elsewhere (*10*). MHE and microwave absorption techniques were applied to measure changes in Hall mobility, conductivity, and charge-carrier density after different pretreatments because they monitor the behavior of ZnO conduction electrons (*11, 12*). Then the ESR spectrometer and a standard ESR cavity were used in their normal mode to detect the presence of paramagnetic species, thus allowing a study of their relationships to the conduction electrons. The adsorption of various gases was also measured to determine the amounts of reversible and irreversible adsorption at 300 K. A comparison of these different results was then used to better understand the bulk processes that occur during the evacuation steps as well as the surface chemistry associated with the adsorption of $O_2$, $H_2$, CO, and $CO_2$ on either evacuated or O-covered ZnO surfaces. Diffuse reflectance FTIR spectroscopy (DRIFTS) was also employed to identify species formed after CO and $CO_2$ adsorption. The availability of this information for the last two molecules could shed light on the role of ZnO in methanol synthesis catalysts (*13*) and water–gas shift catalysts (*14*).

The intent of this study was to identify and quantify the defect sites formed during evacuation, to clarify the chemisorption processes of $O_2$, $H_2$, CO, and $CO_2$ on an evacuated ZnO surface and to examine the interaction between chemisorbed oxygen and the other three molecules. Other possible applications of microwave electrical property measurements include photoluminesence, chemiluminesence, crystallite size effects on dispersed metal particles, and electronic behavior under catalytic reaction conditions.

## EXPERIMENTAL PROCEDURES

A high-purity, high-surface-area ZnO powder was obtained by the decomposition of $ZnCO_3$ prepared by precipitation by mixing a 1 *M* $(NH_4)_2CO_3$ (Aesar, 99.999%) solution with a 1 *M* $Zn(NO_3)_2$ (Aesar, 99.999%) solution. Distilled, deionized water was used. The precipitate was filtered, dried at 393 K in air for a week, then stored in a desiccator. $ZnCO_3$ was decomposed to ZnO inside a quartz cell by heating under vacuum at a rate of 2 K/min to 393 K, and holding for 30 min at 393 K, then heating to 533 K and holding for 30 min, and finally heating to 673 K and holding for 4 h at this maximum temperature. It had a BET surface area of 30 $m^2/g$ and is designated ZnO(I). The ZnO(II) sample was a commercial product (Alfa, 99.99%) and had a surface area of 3.4 $m^2/g$. The same heating procedure was used for ZnO(II) except a rate of 20 K/min was used and the sample was held only 2 h at 673 K.

Gas uptakes were determined in a static volumetric adsorption system utilizing a turbomolecular pump (Balzars, TSU 172) which provides a vacuum of $10^{-7}$ Torr in the sample cell. Pressures were measured by a Baratron sensor head (MKS, model 310). He (MG ind., 99.999%), $O_2$ (MG Ind. 99.999%), $H_2$ (MG Ind., 99.999%), CO (Matheson, 99.99%), and $CO_2$ (MG Ind., 99.99%) were used, and the He, CO, and $H_2$ were further purified by passage through molecular sieve traps and Oxytraps (Alltech Corp.), while the $O_2$ and $CO_2$ were passed through a molecular sieve trap only. After the heat treatment at 673 K, adsorption measurements were performed at 300 K. Unless otherwise specified, after each set of adsorption experiments with a given gas, the sample was reevacuated at 673 K for 2 h, cooled, and the next gas was then adsorbed. The uncertainty of the measured uptakes is $\pm 0.2$ $\mu$mol/g.

The capability to utilize microwave frequencies to measure Hall mobilities and conductivities in a resonant cavity was obtained by modifying an ESR spectrometer (Bruker ER 200D). A new MHE bimodal cavity was constructed from free-cutting brass to replace the ESR cavity. The difference in these two cavities is that the sample is located at the H-field antinode in the ESR

cavity and at the E-field antinode in the MHE cavity. A source modulation method was used with a PIN modulator (H-P 8734B). Experimental conditions of the MHE measurements were: microwave power = 5.0 mW; modulation frequency = 100 kHz, modulation amplitude = 1.0 G; receiver gain = $5 \times 10^4$; and DC magnetic field = 5000 G. A network analyzer (H-P 8720) was used to tune the bimodal cavity and obtain $Q$-factors and resonance frequencies. The details of the modifications and the calculation of Hall mobility and microwave conductivity are given elsewhere (*10–12*). The number of conduction electrons per gram can be calculated from the equation

$$N_c = \frac{\sigma}{\rho e \mu_H} (\mathrm{g}^{-1}), \qquad (1)$$

where $\sigma$ is the conductivity in $(\Omega \cdot \mathrm{cm})^{-1}$, $\mu_H$ is the Hall mobility in $\mathrm{cm}^2/\mathrm{V} \cdot \mathrm{s}$, $e$ is the charge of an electron ($1.6 \times 10^{-19}$ Coulomb), and $\rho$ is the density of zinc oxide (5.606 $\mathrm{g/cm}^3$). The conductivity is determined from microwave cavity measurements using the equation

$$\sigma = 2.78 \times 10^{13} f \left( \frac{Q_0 - Q_L}{Q_0 Q_L} \right) \frac{V_c}{2V_s}, \qquad (2)$$

and the Hall mobility is similarly calculated using the equation

$$\mu_H = \frac{2 \times 10^8}{B} \left( \frac{Q_0}{Q_0 - Q_L} \right) \left( \frac{P_H}{P_1} \right)^{1/2}, \qquad (3)$$

where $f$ is the resonance frequency, $Q_0$ is the unloaded cavity quality factor, $Q_L$ is the quality factor of the cavity with the sample, $V_C$ and $V_S$ are the volumes of the cavity and sample, respectively, $B$ is the DC magnetic field, and $P_H/P_1$ is the ratio of the Hall power transferred to the orthogonal mode to the incident microwave power. Details are given elsewhere (*11, 12*).

The ESR spectra were obtained using a commercial rectangular TE102 ESR cavity (Bruker, ER 4102 ST), a microwave power level of 2.0 mW, and a modulation amplitude of 1.0 G. A weak pitch sample and a sample composed of 1 part DPPH (2,2-Diphenyl-1-Picrylhydrazyl, Chemical Dynamics Corp.) diluted with 1000 parts ZnO were used as references for the calculation of spin concentrations and the calibration of $g$-values (*15, 16*). For the ESR experiments, a 4.0-mm-O.D. quartz tube (Wilmad, 707-SQ) with a high-vacuum valve (Ace Glass, 8195-45) was used to allow evacuation of the ZnO sample, *in situ* pretreatment, and adsorption of the various gases (*10, 12*). The quartz tube was filled with ZnO over a length of approximately 7.5 cm, considerably longer than the cavity size, to avoid any effect due to an inadvertent change in position inside the cavity. This sample tube was connected to the UHV system and evacuated at 673 K for either 4 h or 2 h, then moved *in vacuo* to the ESR cavity where it was connected to the UHV system via $\frac{1}{4}$" copper tubing. Gases were introduced and evacuated through this tubing without moving the tube to eliminate any change in sample position which could affect the ESR measurements.

Diffuse reflectance FTIR spectra of adsorbed CO and $CO_2$ were obtained using a Sirius 100 FTIR spectrometer (Mattson Instruments) equipped with an MCT detector and a modified DRIFTS cell (Harrick Scientific) which was attached to a gas-handling system. A detailed description of the system has been given previously (*17*). $ZnCO_3$ was loaded into the DRIFTS cell and decomposed to ZnO(I) by heat treatment under an Ar flow of 20 $\mathrm{cm}^3$/min. The temperature was raised to 393 K and held for 30 min, increased to 423 K and held for 30 min, then increased to 673 K and held for 4 h. After the sample was cooled to 300 K, a flow of 4 $\mathrm{cm}^3$/min of either $O_2$, CO, or $CO_2$ (120 Torr) was added sequentially to the Ar flow for 30 min before a DRIFTS spectrum was obtained. The sample was then purged for 30 min with Ar and another spectrum was obtained. After the first set of runs with CO the sample was heated for 2 h at 673 K under an Ar flow and cooled before the second set of runs with $CO_2$ was conducted.

TABLE 1

Uptakes of $O_2$, CO, $H_2$, and $CO_2$ on ZnO(I) (30 $m^2/g$) at 20 Torr and 300 K

| Treatment | Adsorption | $\mu$mol gZnO | Molecule $\times 10^{-17}$ g ZnO | Molecule $\times 10^{-17}$ $m^2$ |
|---|---|---|---|---|
| 673 K, Evac. 4 h | 1st $O_2$ | 0.51 | 3.10 | 0.102 |
| | 2nd $O_2$ | 0.13 | 0.78 | 0.026 |
| | Irrev. $O_2$ | 0.38 | 2.3 | 0.76 |
| 673 K, Evac. 2 h | 1st CO | 9.6 | 57. | 1.9 |
| | 2nd CO | 9.3 | 56. | 1.9 |
| | Irrev. CO | 0.3 | 1. | ~0.0 |
| 673 K, Evac. 2 h | 1st $O_2$ | 0.64 | 3.9 | 0.13 |
| | 1st CO | 10.4 | 62. | 2.07 |
| | 2nd CO | 9.7 | 58. | 1.95 |
| | Irrev. CO | 0.7 | 4. | 0.13 |
| 673 K, Evac. 2 h | 1st $H_2$ | 14.3 | 86. | 2.87 |
| | 2nd $H_2$ | 11.2 | 67. | 2.25 |
| | Irrev. $H_2$ | 3.1 | 19. | 0.62 |
| 673 K, Evac. 2 h | 1st $O_2$ | 0.54 | 3.2 | 0.110 |
| | 1st $H_2$ | 13.9 | 84. | 2.79 |
| | 2nd $H_2$ | 12.4 | 75. | 2.49 |
| | Irrev. $H_2$ | 1.5 | 9. | 0.30 |
| 673 K, Evac. 2 h | 1st $CO_2$ | 122. | 730. | 24.5 |
| | 2nd $CO_2$ | 27. | 160. | 5.4 |
| | Irrev. $CO_2$ | 95. | 570. | 19.1 |
| 673 K, Evac. 2 h | 1st $O_2$ | 0.54 | 3.3 | 0.11 |
| | 1st $CO_2$ | 122. | 730. | 24.5 |
| | 2nd $CO_2$ | 34. | 200. | 6.8 |
| | Irrev. $CO_2$ | 88. | 530. | 17.7 |

*Note.* The sample was evacuated at 300 K for 1 h after each adsorption run.

## RESULTS

Oxygen adsorption values on ZnO(I) at 300 K are listed in Table 1. The sample was prepared in the adsorption cell by the decomposition of $ZnCO_3$ under vacuum using the heat treatment procedure described previously, with the final step involving evacuation at 673 K for 4 h. After the initial isotherm of oxygen was obtained, the sample was evacuated at 300 K for 1 h to remove any weakly adsorbed oxygen and the second isotherm was measured. A typical set of isotherms is shown in Fig. 1. Although absolute $O_2$ uptakes were not large, most of the oxygen was irreversibly adsorbed. To obtain uptakes under the same conditions as the MHE and ESR measurements, these isotherms were extrapolated to 20 Torr.

After evacuation at 673 K for 2 h, CO

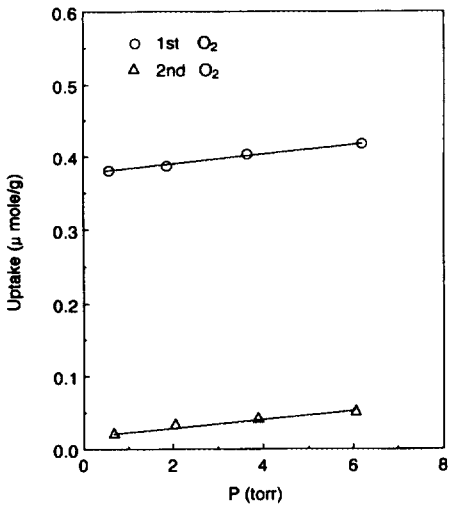


FIG. 1. Oxygen adsorption at 300 K on ZnO(I) after evacuation at 673 K for 4 h.

adsorption was measured at 300 K, as shown in Fig. 2, and uptakes at 20 Torr are given in Table 1. These uptakes are similar to previously reported values (*18*), and the first and second isotherms were essentially identical, indicating that CO adsorbed weakly and reversibly at 300 K. After evacuation at 673 K for 2 h, the oxygen was readsorbed on this surface. The sample was evacuated at 300 K for 1 h, then CO was adsorbed on the oxygen-precovered surface. A small amount of irreversible CO adsorption was now observed, which is attributed to the reaction of CO with chemisorbed oxygen to form a surface carbonate species. Once these species formed, they were not removed by evacuation at 300 K, and the difference in the two CO uptakes represents the amount of CO which reacted with preadsorbed oxygen.

The same experimental procedure was applied to the $H_2$ adsorption measurements, and the uptakes are listed in Table 1. The total uptakes of $H_2$ are similar to those of CO, but there is little change in the amount of irreversible adsorption, indicating no reaction between $H_2$ and chemisorbed oxygen, as discussed later.

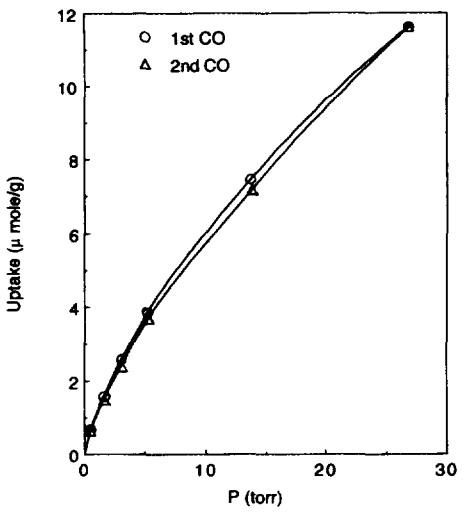


FIG. 2. CO adsorption at 300 K on ZnO(I) after evacuation at 673 K for 2 h.

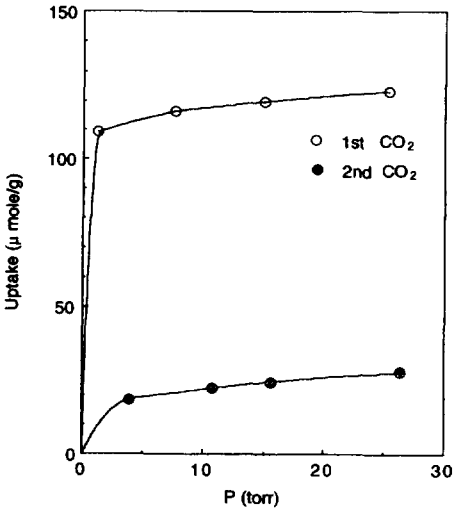


FIG. 3. $CO_2$ adsorption at 300 K on ZnO(I) after evacuation at 673 K for 2 h.

$CO_2$ uptakes were high and a large portion was strongly adsorbed, as shown in Fig. 3. Oxygen preadsorption had no effect on the initial $CO_2$ uptake, and the reversible adsorption increased only slightly. This large irreversible adsorption indicates that $CO_2$ adsorbs on different sites than does $O_2$.

The gas uptakes are summarized in Table 1, and the uptakes are given in $\mu$mol $O_2$, CO, $CO_2$, or $H_2$ per g ZnO, as well as molecules per $m^2$ ZnO. The uptakes are those at 20 Torr because most of the ESR and MHE experiments were performed at that pressure, and these values are compared to the carrier densities measured with the MHE method and the spin concentrations measured by ESR spectroscopy. Oxygen uptakes at 300 K on the lower surface area ZnO(II) sample are listed in Table 2. After evacuation at 673 K for 4 h, the first $O_2$ uptake was 0.2 $\mu$mol/g and the second oxygen uptake was 0.1 $\mu$mol/g. These values are much smaller than those on ZnO(I), due to the lower specific surface area of ZnO(II); uptakes per $m^2$ for the two ZnO samples are similar. The larger oxygen uptakes on the higher surface area zinc oxide indicate that oxygen vacancies are created mostly at the surface.

TABLE 2

Oxygen Uptakes at 20 Torr on ZnO(II) (3.4 $m^2/g$)

| Treatment | Adsorption | Molecules $O_2 \times 10^{-17}$ / g ZnO | Molecule $\times 10^{-17}$ / $m^2$ |
|---|---|---|---|
| 673 K, Evac. 4 h | 1st Isotherm | 1.2 | 0.20 |
| | 2nd Isotherm | 0.6 | 0.10 |
| | Irrev. $O_2$ | 0.6 | 0.10 |

*Note.* Isotherms were extrapolated and uptakes were read at 20 Torr.

The ESR spectra of these zinc oxides were also recorded after various pretreatments and gas exposures to measure spin concentrations, each of which was compared to the number of charge carriers obtained from the corresponding microwave Hall effect and microwave conductivity measurements. All ESR spectra were measured at 300 K. The standard weak pitch sample, which contained 3.3 ppm pitch in KCl, had $10^{13}$ spins per cm in the 4.0-mm-O.D. quartz tube, and it had a $g$-value = 2.0028 with a linewidth of $\Delta H_{pp}$ = 1.7 G (*19*). DPPH was also used as a standard with $g$ = 2.0037, and its spin concentration was calculated from its molecular weight because each molecule has one unpaired electron. A concentration of 1 mg DPPH/g ZnO gave a calculated spin density of $1.5 \times 10^{18}$ spins/g mixture, and the peak intensity agreed with that obtained from the weak pitch signal within 15%. An ESR cavity for x-band frequencies near 9.5 GHz has a sensitivity region about 2 cm in length (*20*), and the same sensitivity length has been measured in our cavity by moving a point sample of DPPH up and down. Consequently, the ESR signal intensity came from the amount of sample located inside this cavity region, and the spin density was obtained by proportioning 2 cm to the total sample length. Spin concentrations were calculated from the expression

$$N_s' = \frac{Y_{pp}'(\Delta H_{pp}')^2}{Y_{pp}(\Delta H_{pp})^2} N_s, \qquad (4)$$

where $N_s$ is the spin concentration, $Y_{pp}$ is the peak-to-peak amplitude of the first-derivative spectrum, and $\Delta H_{pp}$ is the peak-to-peak width of a calibrated standard, while the primed variables represent the measured values for an unknown material (*21*).

Figure 4 shows a typical set of ESR spectra for ZnO(I). $ZnCO_3$ was loaded into a sample cell and decomposed in vacuum by the procedure described earlier. Evacuation at 673 K for 4 h gave a peak at $g$ = 1.9612 ± 0.0004, such as the one shown in Fig. 4a, and oxygen adsorption at 300 K and 0.2 Torr created a new signal at $g$ = 2.0033 ± 0.0001, while it decreased the intensity of the initial peak and shifted it slightly to 1.9600, as shown in Fig. 4b. The signal at $g$ = 2.003 started to broaden at an oxygen pressure of 2.0 Torr, as shown in Fig. 4c. This line broadening has been observed by other groups (*22*), and it is attributed to spin–spin relaxation caused by paramagnetic oxygen weakly adsorbed adjacent to the chemisorbed oxygen species at $g$ = 2.003. Evacuation at 300 K for 30 min restored the sharp signal at $g$ = 2.003, but it did not affect the signal at $g$ = 1.961, as shown in Fig. 4d. The sample was evacuated at 673 K for 2 h, cooled, exposed to 20 Torr oxygen, and then evacuated at 300 K. The surface of zinc oxide was now precovered with strongly adsorbed oxygen, and the ESR spectrum was same as that in Fig. 4d. Exposure to CO at 20 Torr then decreased the signal at $g$ = 2.003 and increased the signal at $g$ = 1.961, as shown in Fig. 4e. This indicates that CO

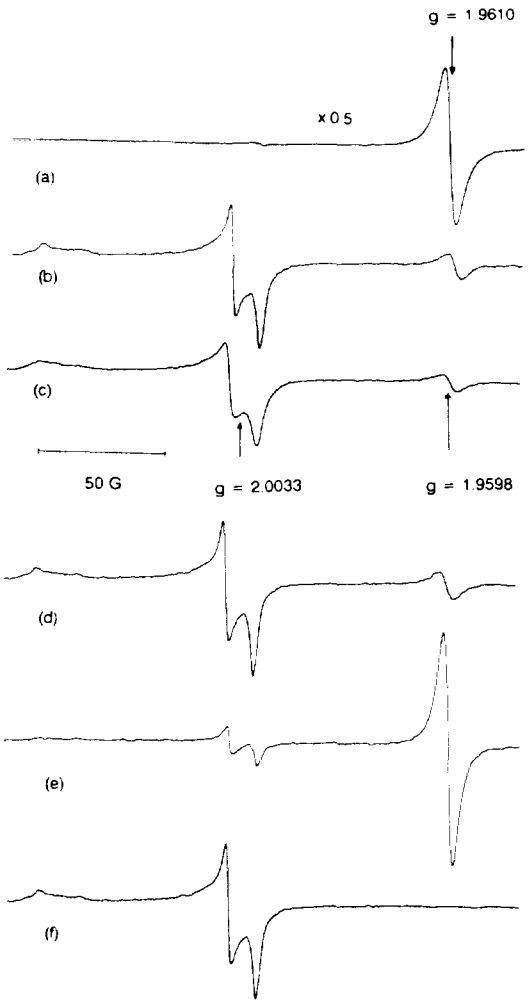


FIG. 4. ESR spectra of ZnO(I): (a) after evacuation at 673 K for 4 h; (b) under 0.2 Torr $O_2$; (c) under 2.0 Torr $O_2$; (d) after evacuation at 300 K for 30 min following $O_2$ exposure; (e) after exposure of O-covered surface such as that in (d) to 20 Torr CO; and (f) after exposure of O-covered surface such as that in (d) to 20 Torr $CO_2$.

reacted with the adsorbed oxygen and paramagnetic oxygen vacancies were restored. The sample was then evacuated at 673 K, cooled, exposed to 20 Torr oxygen, and evacuated at 300 K; a spectrum identical to that in Fig. 4d was again obtained. The sample was now exposed to 20 Torr $CO_2$, which did not affect the signal at $g = 2.003$ but the signal at $g = 1.961$ disappeared, as shown in Fig. 4f. This result indicated that $CO_2$ did not react with chemisorbed oxygen, but chemisorbed $CO_2$ eliminated the oxygen vacancies that remained after oxygen was chemisorbed. It is possible that these remaining vacancy spin centers may not be at the ZnO surface and may have been eliminated by recombination with conduction electrons during $CO_2$ chemisorption.

Table 3 lists the spin concentrations giving the peak at $g = 1.961$ after various treatment conditions of ZnO(I), as calculated from Eq. (4). This spin concentration for ZnO(I) at 300 K was $56 \times 10^{15}$ spins/g after evacuation at 673 K for 4 h, and it decreased to $14 \times 10^{15}$ spins/g after exposure to oxygen at 300 K and 0.02 Torr. As the oxygen pressure increased first to 0.2 and then to 2.0 Torr, the concentration decreased further to $4.5 \times 10^{15}$ and $4.2 \times 10^{15}$ spins/g, respectively. Evacuation at 300 K for 30 min did not change the signal intensity at $g = 1.961$, which indicated that the oxygen adsorbed strongly and irreversibly. After evacuation at 673 K for 2 h the spin concentration increased again, and it decreased after oxygen readsorption. These results were quite reproducible.

After the ZnO(II) sample was evacuated at 673 K for 2 h, it had $11 \times 10^{15}$ spins/g,

TABLE 3

Spin Concentrations of $(V_0^{\cdot})^-$ at $g = 1.961$ for ZnO(I) (Sample 1)

| Sequential treatment | $\Delta H_{pp}$ | $N_s \times 10^{-15}$ (spins/g) |
|---|---|---|
| 673 K, Evac. 4 h | 5.0 | 56.0 |
| 0.02 Torr $O_2$ | 5.0 | 14.0 |
| 0.2 Torr $O_2$ | 6.0 | 4.5 |
| 2.0 Torr $O_2$ | 6.5 | 4.2 |
| 300 K, Evac. 30 min | 6.5 | 4.3 |
| 0.2 Torr $O_2$ | 6.5 | 4.0 |
| 673 K, Evac. 2h | 5.0 | 61.0 |
| 0.02 Torr $O_2$ | 5.5 | 12.0 |
| 0.2 Torr $O_2$ | 5.5 | 6.3 |
| 2.0 Torr $O_2$ | 6.0 | 4.8 |

*Note.* Adsorption was performed at 300 K.

TABLE 4

Spin Concentrations of $(V_0^+)^-$ at $g = 1.961$ for ZnO(II)

| Sequential treatment | $\Delta H_{pp}$ | $N_s \times 10^{-15}$ (spins/g) |
|---|---|---|
| 673 K, Evac. 2 h | 11.0 | 11.0 |
| 0.02 Torr $O_2$ | 6.5 | 2.5 |
| 0.2 Torr $O_2$ | 6.5 | 2.4 |
| 2.0 Torr $O_2$ | 6.5 | 2.2 |
| 300 K, Evac. 30 min | 6.5 | 2.2 |

as listed in Table 4. Oxygen adsorption at 0.02 Torr decreased the spin concentration to $2.5 \times 10^{15}$ spins/g, and increasing the oxygen pressure to 0.2 and 2.0 Torr caused a slight decrease to $2.4 \times 10^{15}$ and $2.2 \times 10^{15}$ spins/g, respectively. Evacuation at 300 K did not change the spin concentration. As discussed previously, oxygen adsorbed on the higher specific surface area ZnO(I) had a greater effect on spin concentrations, which were more dependent on the $O_2$ pressure. The high-surface-area ZnO(I) created more surface oxygen vacancies than ZnO(II) and chemisorbed more oxygen, indicating that the differences between the two ZnO samples are due to the higher percentage of surface vacancies with the higher specific surface area ZnO.

The changes in spin concentration at $g = 1.961$ after $O_2$, CO, $H_2$, and $CO_2$ adsorption are listed in Table 5. A new sample of $ZnCO_3$ was loaded into the sample tube and decomposed to ZnO(I). After evacuation at 673 K for 4 h, the spin concentration was $48 \times 10^{15}$ spins/g and it decreased to $4.1 \times 10^{15}$ spins/g following $O_2$ adsorption at 20 Torr. These results are quite comparable to those in Table 3. When CO was adsorbed on the oxygen-precovered surface, the spin concentration at $g = 1.961$ increased from $3.8 \times 10^{15}$ to $36 \times 10^{15}$ spins/g; however, CO adsorption on this ZnO surface after evacuation at 673 K had no effect on the spin concentration. This indicates that CO reacts with chemisorbed oxygen, presumably to form $CO_2$ or a carbonate species, but adsorbed CO does not affect the surface spin centers formed by evacuation at high temperature.

When $H_2$ was adsorbed on ZnO(I) after evacuation at 673 K, the spin concentration at $g = 1.961$ changed little and no signal was detected at $g = 2.003$. $H_2$ adsorption on an oxygen-precovered surface changed neither the spin concentration produced by chemisorbed oxygen nor that at $g = 1.961$. Even though there was a small irreversible hydrogen uptake, as listed in Table 1, it did not affect any of the detected spin centers. This correlates with the MHE measurements, which also showed no significant effect of $H_2$ on the electrical properties of zinc oxide (*11*, *12*).

After the sample was evacuated at 673 K, $CO_2$ adsorption at 20 Torr decreased the spin concentration at $g = 1.961$ from $48 \times 10^{15}$ to $30 \times 10^{15}$ spins/g. This is a significant decrease even though it was less than that caused by oxygen adsorption. When $CO_2$ was adsorbed on an

TABLE 5

Spin Concentrations and Linewidths of Paramagnetic O Vacancies, $(V_0^+)^-$, at $g = 1.961$ for ZnO(I) (Sample 2) after Adsorption of Different Gases

| Sequential treatment | $\Delta H_{pp}$ Units | $N_s \times 10^{-15}$ (spins/g) |
|---|---|---|
| 673 K, Evac. 4 h | 5.5 | 48. |
| 0.2 Torr $O_2$ | 5.0 | 4.6 |
| 20 Torr $O_2$ | 7.0 | 4.1 |
| 300 K, Evac. 30 min | 6.0 | 3.8 |
| 0.2 Torr CO | 5.0 | 6.5 |
| 20 Torr CO | 4.5 | 36. |
| 673 K, Evac. 2h | 5.5 | 47. |
| 20 Torr CO | 5.5 | 48. |
| 673 K, Evac. 2 h | 5.5 | 48. |
| 0.2 Torr $H_2$ | 5.5 | 49. |
| 20 Torr $H_2$ | 5.5 | 50. |
| 673 K, Evac. 2 h | 5.5 | 48 |
| 20 Torr $O_2$, Evac. 1 h 300 K | 5.5 | 5.7 |
| 0.2 Torr $H_2$ | 5.5 | 5.4 |
| 20 Torr $H_2$ | 5.5 | 5.8 |
| 673 K, Evac. 2 h | 5.5 | 48. |
| 0.2 Torr $CO_2$ | 5.5 | 48. |
| 20 Torr $CO_2$ | 5.5 | 30. |
| 673 K, Evac. 2 h | 5.5 | 53. |
| 20 Torr $O_2$, Evac. 1 h, 300 K | 5.5 | 4.8 |
| 0.2 Torr $CO_2$ | 5.5 | 4.4 |
| 20 Torr $CO_2$ | 8.0 | 0.7 |

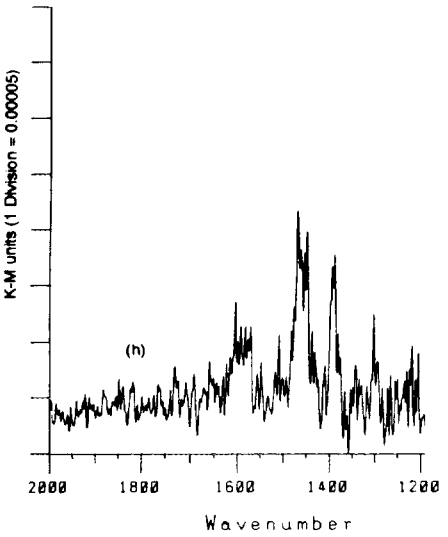


FIG. 5. DRIFTS spectrum of ZnO(I) at 300 K after CO adsorption on an oxygen-covered surface and purging in Ar.

oxygen-precovered surface, the spin concentration at $g = 1.961$ decreased from $4.8 \times 10^{15}$ to $0.7 \times 10^{15}$ spins/g but the signal at $g = 2.003$ did not change, as shown in Fig. 4f. This indicates that $CO_2$ did not interact significantly with preadsorbed oxygen and the adsorption sites for $CO_2$ are different from those for $O_2$.

Diffuse reflectance FTIR was used to identify any surface groups, especially carbonates, that may have been formed on the high-surface-area ZnO after adsorption of the various gases on both a clean evacuated surface and an oxygen-covered surface. No formation of surface species could be detected after evacuation of CO or $CO_2$ with one exception—weak peaks were observed after CO adsorption on an O-covered ZnO surface, as shown in Fig. 5; however, the signal-to-noise ratio was very low. This is not surprising considering the very low concentrations of adsorbed CO from Table 1. Regardless, the four weak bands at 1587, 1458, 1391, and 1299 $cm^{-1}$ do correspond to the peak positions associated with monodentate and bidentate carbonate species (*23*, *24*). The absence of any bands attributable to chemisorbed CO following evacuation is in agreement with previous IR studies (*25*, *26*). After exposure of an evacuated ZnO(I) sample to $CO_2$ and evacuation at 300 K, no bands could be observed; however, under a $CO_2$ pressure of 120 Torr, peaks at 2325, 2348, and 2373 $cm^{-1}$ were obtained after subtraction of the strong gas-phase peaks at 2341 and 2361 $cm^{-1}$, as shown in Fig. 6. These three bands have been previously associated with weakly bound $CO_2$ on ZnO (*27*, *28*).

## DISCUSSION

The carrier densities of zinc oxide were calculated from Eqs. (1) and (2) using the conductivity and Hall mobility results which have been published elsewhere (*11*). The large variations in mobility following different pretreatments found in this study showed the necessity of measuring both electron mobility and conductivity on the

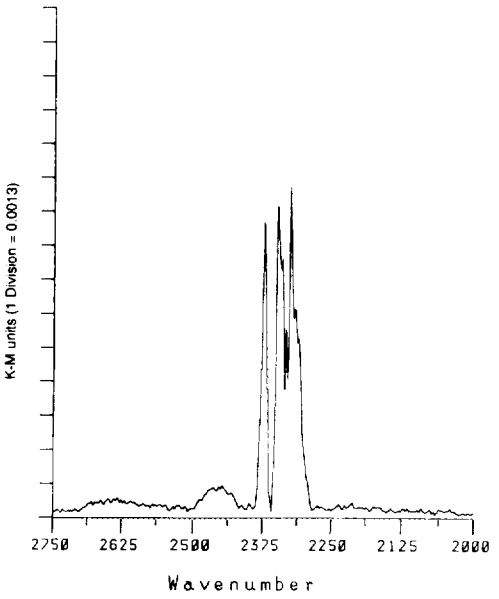


FIG. 6. DRIFTS spectrum of $CO_2$ adsorbed on ZnO(I) at 300 K under 120 Torr $CO_2$ after heating at 673 K for 2 h under flowing Ar, exposing to $O_2$ at 300 K, and then purging with Ar.

TABLE 6

Comparison of Electron Carrier Densities with ESR Spin Concentrations and Adsorption Uptakes for ZnO(1) (Sample 1)

| Treatment | MHE[a] ($e^-$ × $10^{-15}$/g) | ESR (Spins × $10^{-15}$/g) | | Irreversible adsorption (Molec. × $10^{-15}$/g) |
|---|---|---|---|---|
| | | $O_2^-$ | $(V_0^+)^-$ | |
| 673 K, Evac. | 28. | — | 56. | — |
| 20 Torr $O_2$, 300 K Evac. | 0.033 | 74[b] | 4.2 | 230 |
| Change | −28. | +74. | −52. | |
| 673 K, Evac. | 31. | — | 47. | — |
| 20 Torr CO | 26. | — | 48. | ~0 |
| Change | −5. | — | +1. | |
| 673 K, Evac. | | | | |
| 20 torr $O_2$, 300 K Evac. | 0.11 | 39. | 3.8 | — |
| 20 Torr CO | 9. | 7.2 | 36. | 420 |
| Change | +8.9 | −32. | +32. | |
| 673 K, Evac. | 20. | — | 48. | — |
| 20 Torr $CO_2$ | 1.5 | — | 30. | 57,000 |
| Change | −18.5 | — | −18. | |
| 673 K, Evac. | | | | |
| 20 Torr $O_2$, 300 K Evac. | 0.62 | 85. | 4.8 | — |
| 20 Torr $CO_2$ | 0.17 | 85. | 0.7 | 53,000 |
| Change | −0.45 | 0 | −4.1 | |

*Note.* All adsorption conducted at 300 K.

[a] Values taken from Ref. (*11*) and (*12*).

[b] The value is taken at 0.2 Torr $O_2$ pressure because of the line broadening at 20 Torr $O_2$ pressure.

same sample to determine charge carrier density. This is the first application of the MHE method to characterize ZnO electrical properties after various pretreatment conditions and it allows comparisons with ESR spin concentrations and gas uptakes to be used to verify the consistency of the MHE results. The combination of these three data sets also provides insight into ZnO surface chemistry. Comparisons of values from these three different experimental techniques are provided in Table 6 and they are used to develop a model to explain the results.

The evacuation of ZnO at 673 K produced a strong ESR signal at $g = 1.961$ (see Fig. 4a) which has previously been assigned to unpaired electrons at oxygen vacancies, $(V_0^+)^-$, (*1–3*), interstitial zinc ions, $Zn_i^+$, (*29, 30*), or conduction electrons (*15, 22, 31, 32*). The concentrations of $Zn_i^+$ should be extremely low in our experiments because the ESR signal attributed to this species has been found to disappear after a 2-h evacuation at temperatures above 573 K (*1*). Göpel and Lampe have argued that conduction electrons are difficult to detect because of their rapid spin relaxation (*33*); consequently, the most probable assignment of the signal at $g = 1.961$ is to unpaired electrons retained at oxygen vacancies which were created by the loss of lattice oxygen during evacuation at high temperature (*1*). Our nomenclature here is such that a neutral lattice oxygen vacancy, which contains two paired electrons, is represented as $(V_0)^=$; a singly ionized paramagnetic vacancy, which has one associated unpaired electron, is represented as $(V_0^+)^-$; and a doubly ionized lattice oxygen vacancy, which has no electron,

is designated as $(V_0^{2+})^0$; consequently, the net charge on the lattice vacancy is retained and placed inside the parentheses, while the number of electrons associated with it is shown outside the parentheses to clarify the number of electrons associated with each site and to facilitate charge balancing.

Lattice oxygen, $O_{(l)}$, is removed during high-temperature evacuation by desorption of molecular oxygen to create a $(V_0)^=$ site, i.e.,

$$2\,O^=_{(l)} \rightleftharpoons O_2 + 2\,(V_0)^=. \qquad (5)$$

This neutral oxygen vacancy can easily donate an electron to the conduction band of ZnO because of the low ionization energy required (0.04 eV, 1 eV = 24 kcal/mol) (*33*) thereby creating a paramagnetic center, $(V_0^+)^-$:

$$(V_0)^= \rightleftharpoons (V_0^+)^- + e^-. \qquad (6)$$

The formation of the $(V_0^+)^-$ vacancies results in unpaired, localized electrons detectable by ESR spectroscopy quantitatively matched by conduction electrons, $e^-$, which can be characterized by the MHE method; consequently, reaction (6) explains both the high spin concentration at $g = 1.961$ and the increase in conduction electron density of zinc oxide after evacuation at high temperature.

After the high-temperature evacuation step, the zinc oxide had a conduction electron concentration of $28 \times 10^{15}$ $e^-/g$ and a vacancy concentration of $56 \times 10^{15}$ $(V_0^+)^-/g$, as listed in Table 6. The average value of the spin concentration of $(V_0^+)^-$ after evacuation at 673 K (from Tables 3 and 5) is, with its standard deviation (SD), $51 \pm 5 \times 10^{15}$ $(V_0^+)^-/g$ for ZnO(I). These spin concentrations are calculated from the DPPH/ZnO mixture and weak pitch sample, and the uncertainty in calculating absolute spin densities using these reference materials has been reported to be as high as ±30% (*16*). Na calculated electron densities from MHE measurements for several ZnO(I) samples after evacuation at 673 K and obtained an average value, of $24 \pm 5 \times 10^{15}$ $e^-/g$ (*12*). Na *et al.* have tested the MHE change carrier mobility measurement method using Si single crystal semiconductors and achieved values within 30% of the referenced DC mobility values (*10*), thus demonstrating the experimental uncertainty in MHE mobility measurements is not large. The microwave frequency electrical conductivities measured for these same doped Si semiconductors were also within the reference ranges based on the uncertainty of the dopant concentrations, typically ±50% (*12*). Electron density values could have an uncertainty somewhat greater than ±50% in their absolute magnitudes because they are calculated from measured conductivities and measured Hall mobilities. Nevertheless, relative changes in electron densities are expected to be much more accurate. From this cursory accuracy analysis, it is proposed that the absolute values of measured $(V_0^+)^-$ spin concentration and the electron density in ZnO after evacuation at 673 K are within the uncertainty limits for a one-to-one match; for example, from Table 6 the average concentration is $50 \times 10^{15}$ $(V_0^+)^-/g$ ± 30% and the average electron density is $26 \times 10^{15}$ $e^-/g$ ± 50%, and reaction (6) quantitatively accounts for both the ESR and MHE results.

After evacuation of ZnO at 673 K, oxygen adsorption at 300 K produced a new ESR signal near $g_{av} = 2.003$ and decreased the peak height of the $g = 1.961$ signal, as shown in Fig. 1b. This new signal has been assigned in earlier studies to an axially symmetric surface $O^-$ species (*15, 34, 35*) but in more recent studies it has been assigned to an axially symmetric surface $O_2^-$ species (*1, 4–6, 36–38*) or a combination of both (*31, 39*). However, $O_2^-$ is the more probable assignment of the signal at $g_{av} = 2.003$ because isotopic mixing has not been observed during previous $^{18}O_2$ and $^{16}O_2$ adsorption and desorption studies at 295 K (*38*), although evidence of mixing was implied by the hyperfine splitting in ESR spectra from $(^{17}O^{16}O)^-$ species (*4*). One route for oxygen adsorption is the reaction

$$O_2 + (V_0^+)^- \rightarrow [O_2^- - (V_0^{2+})^0], \quad (7)$$

where $[O_2^- - (V_0^{2+})^0]$ represents the paramagnetic $O_2^-$ species adsorbed on a surface oxygen vacancy (*1*). This reaction explains the simultaneous increase of the signal at $g_{av} = 2.003$ and the decrease of the signal at $g = 1.961$, but it does not explain why the electron density also decreases during oxygen adsorption, as shown in Table 6. To explain the latter result, oxygen is assumed to also adsorb on additional surface sites other than oxygen vacancies and interact with conduction electrons to form a paramagnetic $O_{2(s)}^-$ species, as proposed previously (*32*):

$$O_2 + e^- \rightarrow O_{2(s)}^-. \quad (8)$$

Consequently, the formation of $74 \times 10^{15}$ $O_2^-$ species/g almost quantitatively correlates with the disappearance of $52 \times 10^{15}$ $(V_0^+)$ sites/g and $26 \times 10^{15}$ conduction electrons per gram. The irreversible oxygen uptake of $230 \times 10^{15}$ molecule $O_2$/g is three times larger than the quantity of $O_2^-$ species which indicates that there are other sites which can adsorb oxygen in addition to those associated with conduction electrons and $(V_0^+)^-$ centers. For example, it is highly probable that oxygen can interact with $(V_0)^=$ lattice vacancy sites,

$$O_2 + 2\,(V_0)^= \rightarrow 2\,O_{(l)}^=, \quad (9)$$

which is actually the reverse of reaction (5). This is a reoxidation process and the $O_{(l)}^=$ would be a lattice oxygen ion not interacting with ZnO conduction electrons and therefore not ESR active. There is a chance that $O_2^=$ may be formed, but there have been no peroxide species reported in the literature for oxygen adsorption on zinc oxide. Kokes has proposed the presence of $O^=$ on zinc oxide (*15*) and $O^=$ would be the most likely species to fill the original oxygen vacancy sites. The equilibrium constant for reaction (5) could not be found in the literature, but if approximately $80 \times 10^{15}$ molecule $O_2$/g is associated with $O_2^-$ formation via interactions with $(V_0^+)^-$ and $e^-$, then about $150 \times 10^{15}$ molecule $O_2$/g, or about two-thirds of the measured irreversible $O_2$ uptake, would have to be involved in the reoxidation step involving $O^=$.

CO adsorption on ZnO(I) after evacuation had little effect on the ESR signal for $V_0^+$ and essentially no effect on the electron density, as indicated in Table 6. The CO adsorption is completely reversible within experimental uncertainty, in agreement with the study of Gay *et al.* (*40*). The DRIFTS results also indicated no detectable chemisorbed CO either in the presence of gas-phase CO or after purging with Ar. Previous results have shown that CO adsorption occurs with the carbon end toward the zinc oxide surface (*40, 41*), but this bonding is weak and does not involve the transfer of conduction electrons or the interaction with paramagnetic oxygen vacancies.

When CO was adsorbed on an oxygen-precovered surface, the weak ESR signal for $(V_0^+)^-$ increased markedly and the signal for $O_2^-$ decreased significantly, as shown in Fig. 4e. MHE measurements showed that the conduction electron concentration also increased markedly, as shown in Table 6. The adsorption uptakes in Table 1 show that some irreversible CO adsorption now occurred on the ZnO surface. The three sets of results strongly indicate that CO reacts with adsorbed oxygen to increase both the number of paramagnetic oxygen vacancies ($32 \times 10^{15}$/g) and the conduction electron density ($9 \times 10^{15}$/g) and to decrease the paramagnetic oxygen species ($32 \times 10^{15}$/g). Again the sum of the increase in vacancies and conduction electrons is close to the value of the decrease in $O_2^-$ species. The DRIFT spectrum after CO adsorption on this O-covered surface showed weak bands at 1587, 1458, 1391, and 1299 $cm^{-1}$ which did not disappear after the CO was removed (Fig. 5). CO and $CO_2$ adsorption on ZnO has been characterized by IR spectroscopy (*23–28, 42–46*), and the 1587- and 1299-$cm^{-1}$ peaks can be associated with a bidentate carbonate species, while the 1458- and 1391-$cm^{-1}$ peaks are close to those for the

monodentate carbonate species (*25, 26*). Although very weak, these bands are consistent with the ESR, MHE, and adsorption results that indicate CO reacts with surface oxygen. There is one straightforward mechanism by which CO can react with adsorbed oxygen to increase both $(V_0^+)^-$ and $e^-$ concentrations. If CO is oxidized to $CO_2$, then the following steps can be proposed for the $O_2^-$ adsorbed at $(V_0^{2+})^0$ sites:

$$2\,CO + [O_2^- - (V_0^{2+})^0] \rightarrow 2\,CO_{2(ad)} + (V_0^+)^- . \quad (10)$$

This reaction regenerates the paramagnetic $(V_0^+)^-$ species, and it explains the increase of the ESR signal at $g = 1.961$ and the decrease of the signal at $g = 2.003$. A similar reaction can be proposed for the other $O_{2(s)}^-$ species to release conduction electrons:

$$2\,CO + O_{2(l)}^- \rightarrow 2\,CO_{2(ad)} + e^- . \quad (11)$$

This reaction also accounts for a decrease in the ESR signal at $g = 2.003$ as well as the increase in the conduction electron density. These two reactions seem reasonable because the formation of $CO_2$ on zinc oxide surfaces via this route has been reported by Au *et al.* (*41*) and by Allen *et al.* (*47*), and the study of Cheng and Kung has shown that the $CO_2$ formed remains adsorbed at 300 K (*48*). The formation of carbonate could also occur by the reaction

$$CO + 2\,O_{(l)}^= \rightarrow CO_3^= + (V_0)^= , \quad (12)$$

which has no direct effect on $(V_0^+)^-$ and $e^-$ concentrations. If carbonate formation alone was directly responsible for the change in $(V_0^+)^-$ and $e^-$ concentrations, rather than $CO_2$ formation, the most appropriate chemistry would seem to be

$$CO + [O_2^- - (V_0^{2+})^0] + e^- \rightarrow CO_3^= + (V_0^{2+})^0 \quad (13)$$

$$CO + O_{2(s)}^- + e^- \rightarrow CO_3^= . \quad (14)$$

However, although this would remove $O_2^-$ species, it would also reduce the electron density rather than increase it as observed. Therefore, reactions (10) to (12) represent the preferred chemistry controlling the changes in $(V_0^+)^-$ and $e^-$ concentrations.

$CO_2$ adsorption on ZnO(I) after evacuation at 673 K was very large and substantially decreased both the $(V_0^+)^-$ concentration and the electron density. The value of $1.91 \times 10^{18}$ $CO_2/m^2$ compares well with the value of $1.4 \times 10^{18}$ $CO_2/m^2$ reported by Saussey *et al.* for Kadox-15 ZnO (*28*). When $CO_2$ adsorbed on an oxygen-precovered surface, the $(V_0^+)^-$ concentration at $g = 1.961$ decreased further and the electron density also decreased slightly but the $O_2^-$ signal at $g = 2.003$ was not affected. This behavior indicates that the $CO_2$ interacts with oxygen vacancies and the conduction electrons but not with the adsorbed $O_2^-$ species. Adsorption of $CO_2$ on evacuated zinc oxide may occur in a variety of ways; for example, chemisorption on exposed $Zn^{2+}$ cations has been proposed (*30*):

$$CO_2 + Zn_{(cat)} \rightarrow CO_{2(ad)} . \quad (15)$$

This is assumed to be the dominant process because of the large $CO_2$ uptakes, which give coverages greater than 0.1 monolayer (Table 1), and it would explain the nearly equal uptakes on the evacuated and O-covered surfaces. The ratio of charge density relative to the quantity of $CO_{2(ad)}$ is very small, $3.3 \times 10^{-4}$, but is comparable to the value of $3.5 \times 10^{-3}$ reported by Hotan *et al.* for $CO_2$ adsorption on a ZnO single crystal (*49*). It is difficult to account for the decreases in $(V_0^+)^-$ or $e^-$ via a direct interaction with $CO_2$ because a paramagnetic $CO_2^-$ species would presumably be formed and no ESR signal was observed for such a species; in addition, such a species has not been previously identified. A more likely reaction may be between $CO_2$ and the neutral $(V_0)^=$ sites, i.e.,

$$CO_2 + (V_0)^= \rightarrow [CO_{2(ad)} - (V_0)^=] , \quad (16)$$

or possibly

$$CO_2 + (V_0)^= \rightarrow O_{(l)}^= + CO . \quad (17)$$

This could shift the equilibrium represented by reaction (6) and would cause equal decreases in $(V_0^+)^-$ and $e^-$ concentrations. Although the values may be purely fortuitous, the nearly equal changes observed (Table 6) are consistent with this proposal, and the oxygen chemisorption would indicate a surface concentration of $(V_0)^=$ sites = $300 \times 10^{15}$/g [i.e., $(230\text{-}28\text{-}52)(2) \times 10^{15}$], which is close to the measured irreversible $CO_2$ uptake. Another possibility to explain the equal reductions in paramagnetic centers and conduction electrons is the formation of surface carbonate species via the following reaction:

$$2CO_2 + (V_0^+)^- + e \rightarrow CO_3^= + (V_0^{2+})^0 + CO. \quad (18)$$

Additional studies are needed to resolve this chemistry.

There is a significant $O_2^-$ concentration after $O_2$ adsorption on the evacuated ZnO surface that is unaffected by $CO_2$ adsorption, but large decreases in the residual $(V_0^+)$ and $e^-$ concentrations occurred after $CO_2$ adsorption on this surface. Consequently, some of the oxygen vacancies unreactive to molecular oxygen will interact with $CO_2$. It is presumed that the chemistry indicated in reactions (6) and (16) (or possibly (17)) applies, but the order of magnitude difference in absolute values of the decreases in the $(V_0^+)^-$ and e concentrations implies a decoupling of reactions (6) and (16). A small amount of $CO_2^-$ formation, which has been proposed previously but not proven (*2, 41, 50*), could cause a more extensive decrease in $(V_0^+)^-$ concentration via the following reaction:

$$CO_2 + (V_0^+)^- \rightarrow [CO_2^- - (V_0^{2+})^0]. \quad (19)$$

Reversibly adsorbed $CO_2$ species with bands at 2325, 2348, and 2373 $cm^{-1}$ were detected under gas-phase $CO_2$ with DRIFTS, as shown in Fig. 6, but no irreversibly adsorbed $CO_2$ species were observed after removal of the gas-phase $CO_2$. This is inconsistent with the adsorption results and it is not known at this time why the strongly chemisorbed $CO_2$ gave no IR bands. If reaction (17) occurred, no CO bands would be detected because the CO would desorb; however, the large $CO_2$ uptakes in the volumetric adsorption system would not be measured because no pressure change would occur. $CO_2$ adsorption on an oxygen-precovered surface produced no well-defined bands in the 1300–1600 $cm^{-1}$ range (*12*) thus supporting our other results showing that $CO_2$ does not react with the preadsorbed oxygen species.

## SUMMARY

Application of MHE, microwave conductivity measurements, and ESR spectroscopy before and after the adsorption of $O_2$, $CO_2$, CO, and $H_2$ on ZnO provided additional insight into ZnO surface chemistry. Evacuation at 673 K removes lattice oxygen and creates an ESR signal at $g = 1.961$, which has been assigned to a paramagnetic oxygen vacancy, $(V_0^+)^-$, whose formation results from the donation of an electron to the ZnO conduction band. Changes in electron density were calculated from MHE and microwave conductivity measurements. At 300 K some oxygen adsorbs and reduces the concentrations of both $(V_0^+)^-$ and $e^-$ by forming $O_2^-$, while a larger quantity of oxygen appears to reoxidize the lattice in the surface region and remove neutral $V_0$ sites. Reversible CO adsorption occurs on ZnO after evacuation at 673 K, and this weakly adsorbed CO has little effect on the $(V_0^+)^-$ ESR signal or the electron density. However, when CO adsorbs on a surface precovered with oxygen, both the $e^-$ and the $(V_0^+)^-$ concentrations increase significantly while the $O_2^-$ species decrease. The reaction of CO with $O_2^-$ species to form adsorbed $CO_2$ seems to be the most likely explanation of this behavior; carbonate formation did not correlate with the measured changes. $H_2$ adsorption after either evacuation at 673 K or oxygen preadsorption has essentially no effect on either the conduction electrons or the $(V_0^+)^-$ centers. $CO_2$ adsorption

on ZnO after evacuation at 673 K decreases the $e^-$ and $(V_0^+)^-$ concentrations equally, while much smaller decreases occur after adsorption on an oxygen-precovered surface; however, the concentration of the $O_2^-$ species was unaltered. This indicates that $CO_2$ does not react with adsorbed $O_2^-$ species, but can interact with $(V_0^+)^-$ and conduction electrons at sites not covered by molecular oxygen.

## ACKNOWLEDGMENTS

This research was partially supported by the National Science Foundation under Contract CBT85-14723, and by the Florida Power & Light Company. Funding from an NSF Equipment Grant (CBT-8505572) is also gratefully acknowledged. We also thank Paul Fanning for his assistance with the FTIR measurements.

## REFERENCES

1. Morazzoni, F., Scotti, R., and Volontè, S., *J. Chem. Soc. Faraday Trans.* **86,** 1587 (1990).
2. Morazzoni, F., Scotti, R., and Minnaja, N., *J. Chem. Soc. Faraday Trans.* **87,** 493 (1991).
3. Pöppl, A., and Völkel, G., *Phys. Status Solidi A* **115,** 247 (1989).
4. Tench, A. J., and Lawson, T., *Chem. Phys. Lett.* **8,** 177 (1971).
5. Lunsford, J. H., and Jayne, J. P., *J. Chem. Phys.* **44,** 1487 (1966).
6. Sedaka, M., and Kwan, T., *Bull. Chem. Soc. Jpn.* **38,** 1414 (1965).
7. Amigues, P., and Teichner, S. J., *Discuss. Faraday Soc.* **41,** 362 (1966).
8. Glemza, R., and Kokes, R. J., *J. Phys. Chem.* **69,** 3254 (1965).
9. Glemza, R., and Kokes, R. J., *J. Phys. Chem.* **66,** 566 (1962).
10. Na, B. K., Kelly, S. L., Vannice, M. A., and Walters, A. B., *Meas. Sci. Technol.* **2,** 770 (1991).
11. Na, B. K., Vannice, M. A., and Walters, A. B., *Phys. Rev. B* **46,** 12266 (1992).
12. Na, B. K., Ph.D. Thesis, The Pennsylvania State University, 1991.
13. Inoue, T., Iizuka, T., and Tanabe, K., *Bull. Chem. Soc. Jpn.* **60,** 2663 (1987).
14. Shido, T., and Iwasawa, Y., *J. Catal.* **129,** 343 (1991).
15. Kokes, R. J., *J. Phys. Chem.* **66,** 99 (1962).
16. Lunsford, J. H., and Jayne, J. P., *J. Chem. Phys.* **44,** 1492 (1966).
17. Venter, J. J., and Vannice, M. A., *Appl. Spectrosc.* **42,** 1096 (1988).
18. Bolis, V., Fubini, B., Giamello, E., and Reller, A., *J. Chem. Soc. Faraday Trans. 1* **85,** 855 (1989).
19. Poole, C. P., Jr., "Electron Spin Resonance," 2nd ed. Wiley, New York, 1983.
20. Delgass, W. N., Haller, G. L., Kellerman, R., and Lunsford, J. H., "Spectroscopy in Heterogeneous Catalysis." Academic Press, New York, 1979.
21. Wertz, J. E., and Bolton, J. R., "Electron Spin Resonance: Elementary Theory and Practical Applications." McGraw–Hill, New York, 1972.
22. Cope, J. O., and Campbell, I. D., *J. Chem. Soc. Faraday Trans. 1* **69,** 1 (1973).
23. Zawadzki, J., *Chem. Phys. Carbon* **21,** 147 (1989).
24. Hair, M. L., "Infrared Spectroscopy in Surface Chemistry." Dekker, New York, 1967.
25. Tsyganenko, A. A., Denisenko, L. A., Zverev, S. M., and Filimonov, V. N., *J. Catal.* **94,** 10 (1985).
26. Ghiotti, G., Boccuzzi, F., and Scala, R., *J. Catal.* **92,** 79 (1985).
27. Taylor, J. H., and Amberg, C. H., *Can. J. Chem.* **39,** 535 (1961).
28. Saussey, J., Lavalley, J.-C., and Bovet, C., *J. Chem. Soc. Faraday Trans. 1* **78,** 1457 (1982).
29. Codell, M., Gisser, H., Weisberg, J., and Iyengar, R. D., *J. Phys. Chem.* **72,** 2460 (1968).
30. Volodin, A. M., and Cherkashin, A. E., *React. Kinet. Catal. Lett.* **20,** 335 (1982).
31. Wada, T., Kikuta, S., Kiba, M., Kiyozumi, K., Shimojo, T., and Kakehi, M., *J. Cryst. Growth* **59,** 363 (1982).
32. Watanabe, M., *Jpn. J. Appl. Phys.* **19,** 1853 (1980).
33. Göpel, W., and Lampe, U., *Phys. Rev. B* **22,** 6447 (1980).
34. Barry, T. I., and Stone, F. S., *Proc. R. Soc. London A* **255,** 124 (1960).
35. Wong, N. B., Taarit, Y. B., and Lunsford, J. H., *J. Chem. Phys.* **60,** 2148 (1974).
36. Iyengar, R. D., Subba Rao, V. V., and Zettlemoyer, A. C., *Surf. Sci.* **13,** 251 (1969).
37. Setaka, M., Fukuzawa, S., Kirino, Y., and Kwan, T., *Chem. Pharm. Bull.* **16**(7), 1240 (1968).
38. Göpel, W., *Surf. Sci.* **62,** 165 (1977).
39. van Hooff, J. H. C., *J. Catal.* **11,** 277 (1968).
40. Gay, R. R., Nodine, M. H., Henrich, V. E., Zeiger, H. J., and Solomon, E. I., *J. Am. Chem. Soc.* **102,** 6752 (1980).
41. Au, C. T., Hirsch, W., and Hirschwald, W., *Surf. Sci.* **197,** 391 (1988).
42. Denisenko, L. A., Tsyganenko, A. A., and Filimonov, V. N., *React. Kinet. Catal. Lett.* **25,** 23 (1984).
43. Chiorino, A., Ghiotti, G., and Boccuzzi, F., *Vacuum* **41,** 16 (1990).
44. Boccuzzi, F., Ghiotti, G., and Chiorino, A., *J. Chem. Soc. Faraday Trans. 2* **79,** 1779 (1983).

45. Scarano, D., Spoto, G., Zecchina, A., and Reller, A., *Surf. Sci.* **211,** 1012 (1989).
46. Boccuzzi, F., Borello, E., Chiorino, A., and Zecchina, A., *Chem. Phys. Lett.* **61,** 617 (1979).
47. Allen, V. M., Jones, W. E., and Pacey, P. D., *Surf. Sci.* **220,** 193 (1989).
48. Cheng, W. H., and Kung, H. H., *Surf. Sci.* **122,** 21 (1982).
49. Hotan, W., Göpel, W., and Haul, R., *Surf. Sci.* **83,** 162 (1979).
50. Göpel, W., Bauer, R. S., and Hansson, G., *Surf. Sci.* **99,** 138 (1980).